Composition, Structure, Surface Topography, and Electrochemical Properties of Electrophoretically Deposited Nanostructured Fullerene Films†

Wlodzimierz Kutner,*,‡,§ Piotr Pieta,‡ Robert Nowakowski,‡ Janusz W. Sobczak,‡ Zbigniew Kaszkur,‡ Amy Lea McCarty,|| and Francis D'Souza*,||

Institute of Physical Chemistry, Polish Academy of Sciences, 44/52 Kasprzaka, 01-224 Warsaw, Poland, Faculty of Mathematics and Natural Sciences, School of Science, Cardinal Stefan Wyszynski University in Warsaw, Dewajtis 5, 01-815 Warsaw, Poland, and Department of Chemistry, Wichita State University, 1845 Fairmount, Wichita, Kansas 67260-0051

Received April 19, 2005. Revised Manuscript Received July 27, 2005

Nanostructured fullerene films of controlled surface topography have been prepared by electrophoretic deposition from toluene−ethanol mixed solvent solutions. Atomic force microscopy (AFM) imaging of the films revealed that the size of the C_{60} grains could be readily controlled by the time of C_{60} aggregation in bulk solution before deposition and by the strength of the dc electric field applied during the deposition. The deposition was monitored by piezoelectric microgravimetry with the use of an electrochemical quartz crystal microbalance. The mass of the C_{60} film increased exponentially with the time of deposition. The corresponding decrease of the deposition rate with time was presumably due either to the growth of larger C_{60} aggregates in solution of lower mobility or blocking effect of the electrode surface by insulating C_{60} deposits. In the accessible potential window of 0.1 M $(TBA)PF_6$, in acetonitrile, cyclic voltammetry (CV) curves for the C_{60} films featured four cathodic peaks corresponding to four one-electron reductions. Simultaneously recorded multiscan curves of current, resonant frequency change, and dynamic resistance change versus potential for a potential range covering the first two electroreductions, in which the film was relatively stable with respect to dissolution, indicated pronounced transformations in the film caused by the solvent-assisted dynamic equilibria of ions of the supporting electrolyte. However, scanning the potential beyond the second reduction of the fullerene film resulted in a gradual mass decrease due to dissolution of the film. The charge-related piezoelectric microgravimetry, X-ray photoelectron spectroscopy (XPS), and powder X-ray diffraction (XRD) analyses indicated reversible ingress of both TBA^+ counterion and PF_6^- co-ion into the C_{60}^- film. The experimental control over three-dimensional surface assembling of fullerene clusters demonstrated in the present study opens up new avenues to design fullerene electrode materials of high surface area.

1. Introduction

Fullerene films, electrophoretically deposited[1−4] from suspensions of C_{60},[5−12] have recently appeared to be very promising for constructing electrodes for potentially useful applications. For instance, these electrodes can be exploited in photoelectrochemical devices,[13] as relatively thick and porous fullerene electrophoretic films efficiently absorb incident light. Moreover, methanol is readily electrooxidized at electrodes coated with these films, if they are additionally decorated with platinum nanoparticles.[2] Largely developed surface area is responsible for, favorably, high electrooxidation currents at the resulting C_{60}−Pt film electrodes. Hence, miniaturized electrodes for direct methanol fuel cells can be constructed.[2]

Properties of thin films of pristine fullerenes depend on the deposition procedure used.[14,15] That is, different prepara-

† Presented partially at (i) The 19th International Winterschool (Euroconference) on Electronic Properties of Novel Materials. Molecular Nanostructures, Kirchberg in Tirol, Austria, March 12−19, 2005, and (ii) The Electrode Reaction Mechanism and Interfacial Structure (ERMIS 8) Conference, Freudenstadt-Lauterbad, Germany, March 21−April 3, 2005.

* Corresponding authors: e-mail wkutner@ichf.edu.pl (W.K.) or Francis.DSouza@wichita.edu (F.D.).

‡ Polish Academy of Sciences.

§ Cardinal Stefan Wyszynski University in Warsaw.

|| Wichita State University.

(1) Barazzouk, S.; Hotchandani, S.; Kamat, P. V. *Adv. Mater.* **2001**, *13*, 1614.
(2) Vinodgopal, K.; Haria, M.; Meisel, D.; Kamat, P. V. *Nano Lett.* **2004**, *4*, 415.
(3) Barazzouk, S.; Hotchandani, S.; Kamat, P. V. *J. Mater. Chem.* **2002**, *12*, 2021.
(4) Kamat, P. V.; Barazzouk, S.; Hotchandani, S.; Thomas, K. G. *Chem. Eur. J.* **2000**, *6*, 3914.
(5) Wang, Y. M.; Kamat, P. V.; Patterson, L. K. *J. Phys. Chem.* **1993**, *97*, 8793.
(6) Beeby, A.; Eastoe, J.; Heenan, R. K. *J. Chem. Soc., Chem. Commun.* **1994**, 173.
(7) Sun, Y.-P.; Ma, B.; Bunker, C. E.; Liu, B. *J. Am. Chem. Soc.* **1995**, *117*, 12705.
(8) Guldi, D. M.; Hungerbuchler, H.; Asmus, K. D. *J. Phys. Chem.* **1995**, *99*, 13487.
(9) Nath, S.; Pal, H.; Palit, D. K.; Sapre, A. V.; Mittal, J. P. *J. Phys. Chem. B* **1998**, *102*, 10158.
(10) Kamat, P. V.; Thomas, K. G. In *Nanoscale Materials*; Liz-Marzán, L. M., Kamat, P. V., Eds.; Kluwer Academic/Plenum Publishers: Boston, MA, 2003; p 475.
(11) Zhou, S.; Burger, C.; Chu, B.; Sawamura, M.; Nagahama, N.; Toganoh, M.; Hackler, U. E.; Isobe, H.; Nakamura, E. *Science* **2001**, *291*, 1944.
(12) Biju, V.; Barazzouk, S.; Thomas, K. G.; George, M. V.; Kamat, P. V. *Langmuir* **2001**, *17*, 2930.
(13) Kamat, P. V.; Barazzouk, S.; Thomas, K. G.; Hotchandani, S. *J. Phys. Chem. B.* **2000**, *104*, 4014.

10.1021/cm050829i CCC: $30.25
Published on Web 10/15/2005

tion procedures result in different fullerene crystallite sizes and extent of aggregation in the films. Hence, surface topography and, in some instances, solvent and electrolyte entrapments was different. Highly organized densely packed C_{60} films rarely find electrochemical applications because counterions can hardly enter the film during electrochemical oxidation and reduction, thus precluding efficient charge exchange with the electrode substrate.

Other methods of preparation of the fullerene films include vapor sublimation,[16−20] molecular-beam epitaxy,[21,22] solution casting (drop coating, or solvent evaporation),[23−29] abrasive attachment,[30,31] electrochemical oxidation of soluble fullerene anions,[32,33] Langmuir−Blodgett[34−37] or Langmuir−Shäfer[38] transfer of Langmuir films, formation of self-assembled monolayers,[39−47] layer-by-layer assembly,[48−50] and immobilization in surface-confined membranes.[51−60] Surface topography of the resulting C_{60} films varies substantially. That is, molecularly smooth hexagonally packed films[19,25] are prepared on one extreme and highly porous films[1−4] on the other. However, it appeared that topography of the surface-developed fullerene films could be directly controlled so far only by electrophoretic deposition. In this deposition, a C_{60} film is prepared from a suspension of C_{60} aggregates. In general, fullerenes are fairly well soluble in organic solvents of low polarity[61] and form clusters in solvents of high polarity.[62,63] For electrophoretic deposition, therefore, first, C_{60} nanoclusters are allowed to grow in bulk solution of mixed polar and nonpolar solvents, due to strong mutual hydrophobic interactions,[7] to a predefined size. Moreover, this aggregation, performed under carefully adjusted conditions, may lead to formation of spherical fractal C_{60} structures.[64] Next, a constant electric field is applied. In effect, fullerene aggregates gain a partial negative charge, migrate to the target positive electrode, and deposit onto its surface. It appeared that the stronger the electric field applied, the lower the porosity of the resulting film.[1] We show here that the time allowed for C_{60} aggregation in bulk solution before deposition can also be effectively used to control surface topography of the film.

The present work aims at optimizing the conditions for bulk electrophoretic deposition of C_{60} films with respect to the solution composition, aggregation time in bulk solution, and strength of the constant electric field applied. The film deposition was monitored by piezoelectric microgravimetry with the use of an electrochemical quartz crystal microbalance (EQCM). The deposited films were imaged with atomic

(14) Chlistunoff, J.; Cliffel, D.; Bard, A. J. *Thin Solid Films* **1995**, *257*, 166.
(15) Winkler, K.; Costa, D. A.; Balch, A. L. *Pol. J. Chem.* **2000**, *74*, 1.
(16) Kroto, H. W., Fischer, J. E., Cox, D. E., Eds. *Fullerenes*; Pergamon Press: Oxford, U.K., 1993.
(17) Tomura, K.; Nishizawa, M.; Takemura, D.; Matsue, T.; Uchida, I. *Chem. Lett.* **1994**, 1365.
(18) Carlisle, J. J.; Wijayawardhana, C. A.; Evans, T. A.; Melaragno, P. R.; Ailin-Pyzik, I. B. *J. Phys. Chem.* **1996**, *100*, 15532.
(19) Janda, P.; Krieg, T.; Dunsch, L. *Adv. Mater.* **1998**, *10*, 1434.
(20) Leiro, J. A.; Heinonen, M. H.; Laiho, T.; Batirev, I. G. *J. Electron Spectrosc. Relat. Phenom.* **2003**, *128*, 205.
(21) Achiba, Y.; Nakagawa, T.; Matsui, Y.; Suzuki, S.; Shiromaru, H.; Yamauchi, K.; Nishiyama, K.; Kainosho, M.; Hoshi, H.; Maruyama, Y.; Mitani, T. *Chem. Lett.* **1991**, 1233.
(22) Sitter, H.; Nguyen Manh, T.; Stifter, D. *J. Cryst. Growth* **1997**, *174*, 828.
(23) Bhushan, B.; Ruan, J.; Gupta, B. K. *J. Phys. D: Appl. Phys.* **1993**, *26*, 1319.
(24) Marchenko, A.; Cousty, J. *Surf. Sci.* **2002**, *513*, 233.
(25) Uemura, S.; Samori, P.; Kunitake, M.; Hirayama, C.; Rabe, J. *J. Mater. Chem.* **2002**, *12*, 3366.
(26) Miller, B.; Rosamilia, J. M.; Dabbagh, G.; Tycko, R.; Haddon, R. C.; Muller, A. J.; Wilson, W.; Murphy, D. W.; Hebard, A. F. *J. Am. Chem. Soc.* **1991**, *113*, 6291.
(27) Compton, R. G.; Spackman, R. A.; Wellington, R. G.; Green, M. L. H.; Turner, J. *J. Electroanal. Chem.* **1992**, *327*, 337.
(28) Davis, J. J.; Hill, H. A. O.; Kurz, A.; Leighton, A. D.; Safronov, A. Y. *J. Electroanal. Chem.* **1997**, *429*, 7.
(29) Szücs, Á.; Loix, A.; Nagy, J. B.; Lamberts, L. *J. Electroanal. Chem.* **1995**, *397*, 191.
(30) Suárez, M. F.; Marken, F.; Compton, R. G.; Bond, A. M.; Miao, W.; Raston, C. L. *J. Phys. Chem. B* **1999**, *103*, 5637.
(31) Bond, A. M.; Miao, W.; Raston, C. L. *J. Phys. Chem. B* **2000**, *104*, 2320.
(32) Koh, W.; Dubois, D.; Kutner, W.; Jones, M. T.; Kadish, K. M. *J. Phys. Chem.* **1993**, *97*, 6871.
(33) Koh, W.; Dubois, D.; Kutner, W.; Jones, M. T.; Kadish, K. M. *J. Phys. Chem.* **1992**, *96*, 4163.
(34) Jehoulet, C.; Obeng, Y. S.; Kim, Y. T.; Zhou, F. M.; Bard, A. J. *J. Am. Chem. Soc.* **1992**, *114*, 4237.
(35) Uemura, S.; Ohira, A.; Ishizaki, T.; Sakata, M.; Kunitake, M.; Taniguchi, I.; Hirayama, C. *Chem. Lett.* **1999**, 279.
(36) Luo, C. P.; Huang, C. H.; Gan, L. B.; Zhou, D. J.; Xia, W. S.; Zhuang, Q. K.; Zhao, Y. L.; Huang, Y. Y. *J. Phys. Chem. B* **1996**, *100*, 16685.
(37) Zhang, W.; Shi, Y.; Gan, L.; Huang, C.; Luo, H.; Wu, D.; Li, N. *J. Phys. Chem. B* **1999**, *103*, 675.
(38) Conoci, S.; Guldi, D. M.; Nardis, S.; Paolesse, R.; Kordatos, K.; Prato, M.; Ricciardi, G.; Vicente, M. G. H.; Zilbermann, I.; Valli, L. *Chem. Eur. J.* **2004**, *10*, 6523.
(39) Chen, K.; Caldwell, W. B.; Mirkin, C. A. *J. Am. Chem. Soc.* **1993**, *115*, 1193.
(40) Caldwell, W. B.; Chen, K. M.; Mirkin, C. A.; Babinec, S. J. *Langmuir* **1993**, *9*, 1945.
(41) Shi, X.; Caldwell, W. B.; Chen, K.; Mirkin, C. A. *J. Am. Chem. Soc.* **1994**, *116*, 11598.
(42) Allemand, P. M.; Khemani, K. C.; Koch, A.; Wudl, F.; Holczer, K.; Donowan, S.; Gruner, G.; Thompson, J. D. *Science* **1991**, *253*, 301.
(43) Amihood, D.; Katz, E.; Willner, I. *Langmuir* **1995**, *11*, 1313.
(44) Creager, S. E.; Collard, D. M.; Fox, M. A. *Langmuir* **1990**, *6*, 1617.
(45) Lahav, M.; Gabriel, T.; Shipway, A. N.; Willner, I. *J. Am. Chem. Soc.* **1999**, *121*, 258.
(46) Imahori, H.; Azuma, T.; Ajavakom, A.; Norieda, H.; Yamada, H.; Sakata, Y. *J. Phys. Chem. B* **1999**, *103*, 7233.
(47) Arias, F.; Godinez, L. A.; Wilson, S. R.; Kaifer, A. E.; Echegoyen, L. *J. Am. Chem. Soc.* **1996**, *118*, 6086.
(48) Guldi, D. M.; Pellarini, F.; Prato, M.; Granito, C.; Troisi, L. *Nano Lett.* **2002**, *2*, 965.
(49) Luo, C. P.; Guldi, D. M.; Maggini, M.; Menna, E.; Mondini, S.; Kotov, N. A.; Prato, M. *Angew. Chem., Int. Ed.* **2000**, *39*, 3905.
(50) Liu, Y.; Wang, Y.; Lu, H.; Claus, R. O. *J. Phys. Chem. B* **1999**, *103*, 2035.
(51) Nakashima, N.; Kuriyama, T.; Tokunaga, T.; Murakami, H.; Sagara, T. *Chem. Lett.* **1998**, 633.
(52) Nakashima, N.; Nonaka, Y.; Nakanishi, T.; Sagara, T.; Murakami, H. *J. Phys. Chem. B* **1998**, *102*, 7328.
(53) Nakashima, N.; T., T.; Nonaka, Y.; Nakanishi, T.; Murakami, H.; Sagara, T. *Angew. Chem., Int. Ed.* **1998**, *37*, 2671.
(54) Nakanishi, T.; Murakami, H.; Sagara, T.; Nakashima, N. *J. Phys. Chem. B* **1999**, *103*, 304−308.
(55) Nakanishi, T.; Murakami, H.; Sagara, T.; Nakashima, N. *Chem. Lett.* **2000**, 340.
(56) Nakashima, N.; Ishii, T.; Shirakusa, M.; Nakanishi, T.; Murakami, H.; Sagara, T. *Chem. Eur. J.* **2001**, *7*, 1766.
(57) Nakashima, N.; Wahab, N. W. B.; Mori, M.; Murakami, H.; Sagara, T. *Chem. Lett.* **2001**, 748.
(58) Song, F.; Echegoyen, L. *J. Phys. Chem. B* **2003**, *107*, 5844.
(59) Nakanishi, T.; Ohwaki, H.; Tanaka, H.; Murakami, H.; Sagara, T.; Nakashima, N. *J. Phys. Chem. B* **2004**, *108*, 7754.
(60) Nakashima, N. In *Encycl. Nanosci. Nanotechnol.* **2004**, *3*, 545−556.
(61) Ruoff, R. S.; Tse, D. S.; Malhotra, R.; Lorents, D. C. *J. Phys. Chem.* **1993**, *97*, 3379.
(62) Sun, Y. P.; Bunker, C. *Nature* **1993**, *365*, 398.
(63) Alargova, R.; Deguchi, S.; Tsujii, K. *J. Am. Chem. Soc.* **2001**, *123*, 10460.
(64) Bulavin, L. A.; Adamenko, I. I.; Yashchuk, V. M.; Ogul'chansky, T. Y.; Prylutskyy, Y. I.; Durov, S. S.; Scharff, P. *J. Mol. Liq.* **2001**, *93*, 187.

force microscopy (AFM) in order to determine their surface roughness and size of the C_{60} surface structures. With simultaneous measurement of multiscan cyclic voltammetry (CV) curves and changes of both resonant frequency and dynamic resistance of the film-coated quartz resonator, the electrochemical behavior of the films composed of C_{60}^{n-} ($n = 1, 2$) anions and, particularly, transformations in the films accompanied by solvent-assisted ingress and egress of ions of the supporting electrolyte was investigated. Moreover, X-ray photoelectron spectroscopy (XPS) and powder X-ray diffraction (XRD) analyses performed were helpful to address elemental composition and structure aspects, respectively, of the freshly prepared, electroreduced and back-electrooxidized C_{60} films. As demonstrated herein, experimental control over three-dimensional surface assembling of fullerene clusters was possible by the present electrophoretic technique.

2. Experimental Section

2.1. Chemicals. C_{60} (99.5% purity) was from M. E. R. Corp. (Tucson, AZ). Toluene (pro analysis) of Chempur (Piekary Slaskie, Poland) and acetonitrile (≥99.5% purity, $H_2O \leq 0.001$) of Fluka were deaerated before measurements with a solvent-saturated argon purge. Line ethanol, containing rectified ethyl alcohol (96.3 wt %) and diethyl ether (3.7 wt %), was from Linegal Chemicals Co., Ltd. (Warsaw, Poland). Tetra(*n*-butyl)ammonium hexafluorophosphate, (TBA)PF_6, (puriss, electrochemical grade, ≥99.0%) was from Fluka. Methylene chloride (pro analysis) was from Chempur (Piekary Slaskie, Poland). All chemicals were used as received.

2.2. Apparatus. For electrophoretic deposition, a two-electrode system was used, which consisted of a 1×1 cm^2 Pt tab and Pt film electrode serving as the auxiliary (negative) and working (grounded) electrode, respectively. The Pt film electrodes were cathodically sputtered onto the 14-mm diameter quartz resonators. The electrode diameter of the 5- and 10-MHz resonator was 5 and 6 mm, respectively. A dc voltage was applied to the electrodes by using a stabilized power supply type IZS-5/71 of INCO (Warsaw, Poland). Simultaneously with electrophoretic deposition of C_{60} films, piezoelectric microgravimetric experiments were performed by use of an electrochemical quartz crystal microbalance type EQCM 5710 of the Institute of Physical Chemistry (Warsaw, Poland) under EQCM 5710-S2 software control. This microbalance allowed simultaneous measurement of changes of current, resonant frequency, and dynamic resistance of a 10-MHz quartz resonator. C_{60} fine powder was dissolved in toluene in an ultrasonic bath type UM-0.5 of Techpan (Warsaw, Poland). An Autolab computerized electrochemistry system of Eco Chemie (Utrecht, The Netherlands) was used for CV measurements. This system was equipped with a PGSTAT20 potentiostat and controlled by the GPES 4.9 software of Eco Chemie. A glass three-electrode conically tapered electrochemical cell was used with Pt/quartz, Pt tab, and Ag wire serving as the working, auxiliary, and pseudoreference electrode, respectively.

High-resolution topographical analysis of surfaces of the electrophoretically deposited C_{60} films was performed in air by AFM with a scanning probe microscopy (SPM) instrument, viz., TMX 2000 Discoverer microscope of TopoMetrix (Santa Clara CA). Topography of the films was examined in both the noncontact and constant force modes. The silicon probes and two standard $x-y$ scanners of the 25×25 μm^2 and 70×70 μm^2 range (all from TopoMetrix) were applied. Several images of various areas and magnifications were collected for each film in order to gain better understanding of surface topography developed under different deposition conditions.

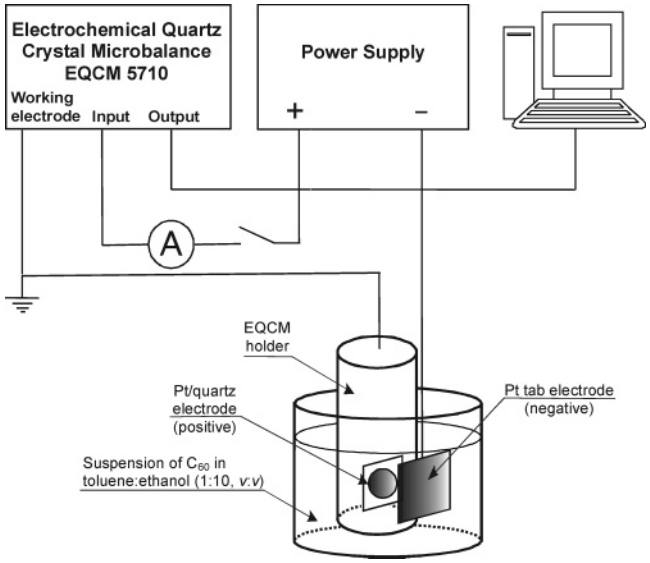

Figure 1. Schematic view of the experimental setup for electrophoretic deposition of a C_{60} film on a Pt/quartz electrode and simultaneous monitoring of the film growth by use of electrochemical quartz crystal microbalance.

The XPS spectra were recorded with an Escalab-210 spectrometer of VG Scientific (East Grinstead, U.K.) by use of Al Kα ($h\nu$ = 1486.6 eV) X-ray radiation. The pressure in the spectrometer chamber was $\sim 5 \times 10^{-9}$ mbar. High-resolution scans were recorded with the 20 eV analyzer pass energy at a 0.05 eV increment for the C 1s core level spectrum and a 0.1 eV increment for the N 1s, F 1s, and P 2p core level spectra. The analyzer axis was normal to the surface. The spectra were analyzed by the Avantage data system software of Thermo Electron (East Grinstead, U.K.) using a Gauss-to-Lorentz constant ratio of 0.3. The spectra were corrected for background by the Shirley method.[65]

The XRD patterns were recorded with a Siemens D5000 powder diffractometer of Bruker AXS GmbH (Karlsruhe, Germany) with a sealed-off Cu tube, which provided Kα X-ray radiation of λ = 0.154 184 nm. A scintillation detector, standard setting of the optics with a Ni filter, and a laboratory-made flow-through camera allowing for in situ measurements under inert gas atmosphere were used. The fullerene film samples, deposited onto Pt/quartz resonators for EQCM, were transferred to the camera in about 1 min after being taken away from the argon-filled electrochemical cell. The camera was fed with helium (N5.0) of a constant flow rate of 20 mL min^{-1}. Asymmetric geometry was adopted for the measurements in order to maximize the X-ray beam intensity scattered by the examined fullerene film. In this geometry, the angle of the incident beam was set constant at 1°. The preliminary test measurements were performed for a number of incident beam angles in order to avoid any parasitic reflection that might originate from either the quartz support or the platinum film electrode. Because of low intensity of the diffracted X-ray radiation, patterns for the fullerene films were acquired for ca. 24 h.

2.3. Procedures. An experimental setup for bulk electrophoresis is depicted in Figure 1. The Pt electrodes were polarized with 50 V dc unless stated otherwise. This voltage appeared to be the most suitable for relatively slow and, therefore, easy to control deposition of the C_{60} films. Distance between the two Pt electrodes was kept constant at 4 mm throughout all the measurements. Before deposition of C_{60} films, the Pt/quartz resonators were cleaned by soaking in a toluene−acetonitrile (1:1 v/v) solution for at least 2 h and then rinsed with ethanol. Appropriate weight portion of a C_{60}

(65) Shirley, A. D. *Phys. Rev. B* **1972**, *5*, 4709.

fine powder was dissolved under sonication in deaerated toluene to yield a 0.1 mM C_{60} solution. As opposed to earlier investigations where mixed solvent solutions of acetonitrile and toluene were used for C_{60} aggregation, resulting in rapid formation of the C_{60} suspension,[1−4] here the C_{60} suspension was prepared by mixing a sample of the 0.1 M C_{60} toluene solution with deaerated line ethanol at the toluene-to-ethanol ratio of 1:10 (v/v). This ratio was used throughout all the present investigations because it afforded relatively slow aggregation and, therefore, was most suitable for its convenient control. The time that elapsed between mixing the solutions and application of the dc voltage was kept constant at 1 min unless stated otherwise. The total time of each deposition did not exceed 15 min. During this time, the fullerene film was deposited and the frequency change was measured. After ca. 12 min of deposition, the frequency change became negligibly small, indicating that deposition was seized despite the fact that the fullerene suspension in solution was not much depleted, as opposed to earlier studies.[1−4]

The C_{60} films, electrophoretically deposited onto Pt/quartz electrodes, and the deaerated 0.1 M $(TBA)PF_6$ acetonitrile solution were subsequently used for simultaneous CV and piezoelectric microgravimetric investigations.

In our early electrophoretic deposition experiments, quartz crystal resonators with vapor-deposited gold-over-chromium or gold-over-titanium film electrodes were used. Unfortunately, the gold films readily peeled off from surfaces of the quartz wafers after high dc voltage was applied, thus precluding any further piezoelectric microgravimetric experiments.

For AFM imaging, the C_{60} films were deposited by electrophoresis onto the surfaces of highly oriented pyrolytic graphite (HOPG) disks. A 1 × 1 cm^2 platinum tab and 4 mm in diameter HOPG disk served as the auxiliary (negative) and working (grounded) electrode, respectively. The electrodes were separated by 4 mm. A dedicated PTFE holder for the HOPG disk was used for this deposition. Samples, allowed to aggregate in solution for 4 min (referred to as short-time aggregation) and 12 min (long-time aggregation), were prepared by subsequent 2-min electrophoretic deposition at 50 or 100 V dc voltage applied.

For the XPS and powder XRD analyses, fresh C_{60} films were prepared by electrophoretic deposition onto the surfaces of the 5-MHz Pt/quartz crystal resonators, similar to the films deposited for the EQCM studies. After deposition, the films were thoroughly rinsed with argon-deaerated acetonitrile and stored in an argon atmosphere before analysis.

All experiments were performed at ambient temperature (22 ± 1) °C.

3. Results and Discussion

First, by piezoelectric microgravimetry, we investigated electrophoretic deposition of C_{60} films. Then the resulting films were imaged by AFM and their electrochemical properties were examined by performing simultaneously CV and piezoelectric microgravimetric experiments. Finally, the XPS compositional and XRD structural analyses were performed.

3.1. Electrophoretic Deposition of C_{60} Films. Electrophoretic deposition of C_{60} films was investigated by piezoelectric microgravimetry. Curve 1 in Figure 2 shows dependence of the resonant frequency change, Δf, on time for the deposition averaged over results obtained for five different 5 MHz Pt/quartz resonators. For the initial 15 s after mixing of 0.1 mM C_{60} toluene solution and line ethanol,

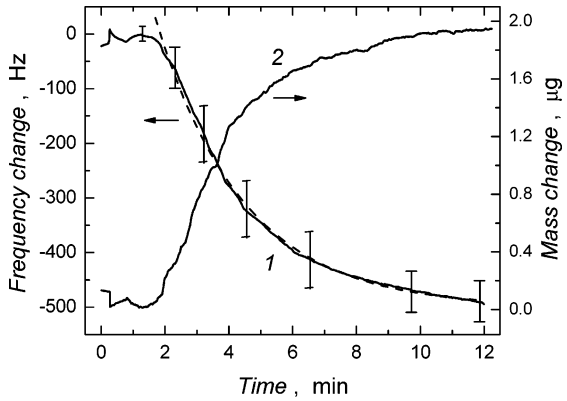

Figure 2. (Curve 1) Mean frequency change with time for electrophoretic deposition of C_{60} films on 5-MHz Pt/quartz electrodes from a mixed solvent solution of a toluene-to-ethanol ratio of 1:10 (v/v) (solid curve; vertical bars stand for standard deviations) and exponential fit (dashed curve). (Curve 2) Time dependence of the mass change of the electrodes, recalculated from data in curve 1 by use of the Sauerbrey equation.

C_{60} suspension was allowed to grow at open circuit, that is, the electrodes were not polarized with external dc voltage and, consequently, a C_{60} film was not deposited. Then dc voltage was switched on and, in effect, a positive spike was reproducibly formed in the Δf vs t transient. This spike was followed by a shallow minimum, after which a small flat maximum was developed at ca. 75 s. Next, after a total of ca. 120 s, a C_{60} film commenced to deposit while the solution became progressively more turbid due to the growth of larger C_{60} aggregates. The film deposition was manifested by the decrease of the resonant frequency with time (curve 1 in Figure 2). With the use of the Sauerbrey equation

$$\Delta f = \frac{-2 f_0^2 \Delta m}{A(\mu_Q \rho_Q)^{1/2}} \tag{1}$$

(where Δf is the resonant frequency change, Δm is the mass change of a quartz resonator, $\mu_Q = 2.947 \times 10^{11}$ dyn cm^{-2} is the shear modulus of quartz, $\rho_Q = 2.648$ g cm^{-3} is the quartz density, A is the acoustically active area of a quartz resonator, and f_0 is the fundamental frequency of the quartz resonator), this frequency change was recalculated into the mass change (curve 2 in Figure 2). This mass change increased exponentially with time. The decaying portion of the Δf vs t curve was exponentially fitted, $\Delta f = A_1 \exp(t/t_1) + \Delta f_0$, with the parameters $\Delta f_0 = -500.151\,93$ Hz, $A_1 = 983.409\,24$ Hz, and $t_1 = -164.520\,27$ s and correlation coefficient $R^2 = 0.997$. Unlike many-day aggregation leading to formation of C_{60} fractal nanoclusters in solution,[64] the present exponential dependence of mass deposition on time implies that films composed of nonfractal C_{60} structures were deposited. The total mean mass of these films deposited after 12 min was about 1.7 μg. The estimated thickness and coverage of a monolayer film of hexagonally packed C_{60} pseudospheres are about 0.87 nm and 1.43×10^{-7} g cm^{-2} and 0.87 nm, respectively. Hence, estimated mean thickness of the film obtained here did not exceed $d \approx 53$ nm and electrode coverage was $\Gamma \approx 1.2 \times 10^{-8}$ mol cm^{-2}, indicating that the films were composed of ca. 61 equivalent monolayers. Noticeably, this mean thickness, determined by microgravimetry, is almost an order of magnitude lower than

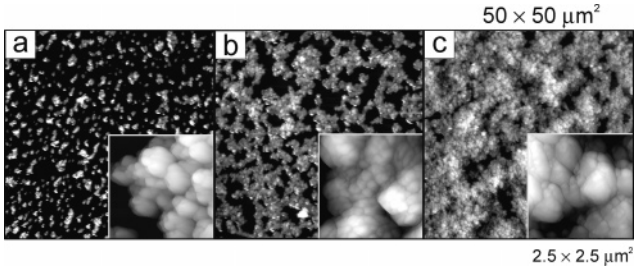

Figure 3. Atomic force microscopic images, at 50 × 50 μm^2 magnification, of C_{60} films electrophoretically deposited on the highly oriented pyrolytic graphite electrodes for (a) short-time (4-min) aggregation followed by 2-min deposition at 50 V dc, (b) long-time (12-min) aggregation followed by 2-min deposition at 50 V dc, and (c) short-time (4-min) aggregation followed by 2-min deposition at 100 V dc from mixed solvent solutions of a toluene-to-ethanol ratio of 1:10 (v/v). (Insets) Fragments of the same films are shown under higher 2.5 × 2.5 μm^2 magnification.

the effective thickness of fullerene domains in films, determined by AFM (see section 3.2).

From the slope of the Δm vs t curve (curve 2 in Figure 2), the rate of the film deposition was determined. That is, the initial rate was 6.9 ng s^{-1}, being subsequently maintained for ca. 4 min. Then this rate gradually decreased and it was over 1 order of magnitude smaller and equal to 0.68 ng s^{-1} in the final stage of deposition. Over the 2−12 min time interval, a mean rate of the mass increase was 2.4 ng s^{-1}. This rate decrease with time might be caused by at least two effects. One might arise from the growth in solution of the fullerene aggregates of larger sizes with time and, hence, decrease of their mobility. Consequently, ability of their deposition might decrease. Apparently small and large aggregates were initially and finally deposited, respectively. The other effect (see section 3.2) might be due to the insulating properties of the deposited C_{60} film and, hence, surface blocking effect. While being quite well redox-conductive (see section 3.3), the C_{60} film is electronically insulating. Therefore, the effective dc electric field causing migration of the fullerene aggregates in solution toward the electrode surface might be decreased due to the ohmic potential loss across this highly resistive film.[32]

3.2. Surface Topography of the Electrophoretically Deposited C_{60} Films. The AFM imaging of surfaces of the C_{60} films prepared by electrophoresis on the HOPG electrodes at short and long aggregation times as well as at 50 and 100 V dc applied provided information on the shape and size of the deposited fullerene nanostructures and surface coverage, as well as the film thickness and roughness.

Importantly, spherical deposits (Figure 3) with the 200−250 nm diameter microscopically distinguishable C_{60} clusters were obtained under all deposition conditions applied. This cluster diameter was larger than that of clusters obtained in earlier electrophoretic depositions,[1−4] presumably because time allowed for the cluster formation in bulk solution in the present studies was longer. All the clusters coalesced to form larger aggregates. It could be that these aggregates were already formed in solution before deposition. Most likely, the aggregates that approached the electrode by migration were deposited on the bare electrode surface available. Such a deposition scenario might be due to insulating property of the C_{60} film formed. The ohmic potential drop across this film contributed to the decrease of the effective local electric field in solution.[32] Hence, the migration rate of the aggregates in solution in the vicinity of the deposited aggregates was decreased. Therefore, the aggregates coated progressively the bare surface in the course of deposition and then welded together to form larger domains.

For deposition at 50 V dc, an average aggregate diameter was 600−700 nm, for both the short- (Figure 3a) and long-time (Figure 3b) aggregation. However, individual clusters were resolved best in aggregates obtained during long-time aggregation at 50 V dc (Figure 3b), pointing to aggregation in solution rather than on the surface. Moreover, height of the aggregates was similar for both short- and long-time aggregation and close to 440−550 nm. Furthermore, the mean height of surface domains, considered as the film thickness, was similar for short- and long-time aggregation and close to 500 nm, indicating that the films were built of mono- rather than multiaggregate layers. However, the mean surface coverage differed markedly. That is, it was close to 50% and 75% for short- and long-time aggregation, respectively. Presumably, the cluster concentration in solution was controlled by the aggregation time, but the size of the aggregates deposited on the electrode was controlled by the magnitude of dc voltage applied (see below). Therefore, the size of the aggregates deposited at 50 V dc was similar but surface coverage varied for different time intervals of aggregation.

The AFM topographical analysis also allowed us to determine the number of domains per examined area. It appeared that for 50 V dc there were 54 and 3 domains in the 20 × 20 μm^2 area imaged and 210 and 13 domains in the 50 × 50 μm^2 area for short- and long-time aggregation, respectively. These numbers indirectly reflect the extent of the domain coalescence. The AFM technique allows for counting the number of separate objects seen on the imaged surface. In the case of coalescence, the resulting larger objects are counted as one object. From our results, it followed that there were 600−700 nm diameter domains separated one from the other for short-time aggregation. For long-time aggregation, domains of similar size were obtained but they were welded. Therefore, the number of these domains was lower.

For deposition at 100 V dc and short-time aggregation (Figure 3c), the aggregate size was much larger than that obtained at 50 V and close to 700−1500 nm. Apparently, higher electric field forced larger aggregates, formed in solution, to migrate to the electrode surface. This migration, resulting in an almost pinhole-free continuous film of surface coverage close to 95%, was much more efficient than that at 50 V dc. However, the film thickness was 500−700 nm, as if the aggregates were orientated flat on the surface.

Importantly, surface roughness of the films, $R_{sa} = A_{3D}/A_{2D}$, represented by the ratio of area in three-dimensional space, A_{3D}, to that projected into two-dimensional space, A_{2D}, was different for different conditions of deposition. The determined R_{sa} data are presented as a function of imaging resolution, that is, pixel size, in Figure 4. As expected, the R_{sa} values for high coverage and small number of domains per examined area were lower than those for low coverage and large number of domains. In particular, relatively high

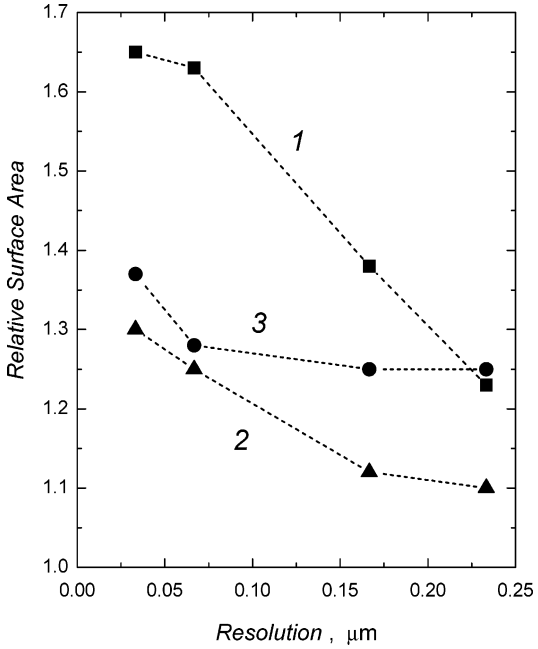

Figure 4. Dependence of relative surface area on resolution, that is, pixel size, for the atomic force microscopic images of C_{60} films electrophoretically deposited on electrodes of highly oriented pyrolytic graphite for (1) short-time (4-min) aggregation followed by 2-min deposition at 50 V dc, (2) long-time (12-min) aggregation followed by 2-min deposition at 50 V dc, and (3) short-time (4-min) aggregation followed by 2-min deposition at 100 V dc in mixed solvent solutions of a toluene-to-ethanol ratio of 1:10 (v/v).

R_{sa} values were obtained for short-time aggregation and lower dc voltage applied (curve 1 in Figure 4), indicating formation of porous films. As anticipated, the R_{sa} dependence on resolution was much more pronounced for films formed after short- rather than long-time aggregation and at lower rather than higher dc voltage applied (curve 1 in Figure 4). Apparently, the surface aggregates were welded together to form larger domains covering both more continuously and smoothly the examined surface for longer aggregation time and higher voltage.

3.3. Transformations in the Films Accompanying Electrode Processes of C_{60}. Counterions, like tetraalkylammonium cations[32,66,67] and metal cations even to a greater extent,[29,68] are responsible for stabilization of reduced C_{60} films with respect to oxidation, making the electrode processes highly irreversible. Pronounced, exceeding 550 and 300 mV for the C_{60}^0/C_{60}^- and C_{60}^-/C_{60}^{2-} redox couples, respectively, cathodic-to-anodic CV peak potential differences manifest this irreversibility. Moreover, electrochemically induced ingress of TBA^+ results in crystallographic changes of vapor-deposited C_{60} films.[17]

Highly reduced C_{60} films are unstable with respect to dissolution in polar aprotic solvent solutions[32,33] and C_{60}^{2-} is readily dissolved, for instance, in dimethylformamide−water mixed solvent solution[69] but only slightly in acetonitrile.[32] Therefore, to get closer insight into electrochemical properties of the electrophoretically deposited C_{60} films, we used acetonitrile as solvent and imposed such a limit on the negative reversal potential that only the first two cathodic and the related two anodic CV peaks were developed (Figure 5). Electroreduction and subsequent electrooxidation of the film, accompanied by the counterion dynamic equilibrium, must cause changes in the film swelling with the acetonitrile solvent. These changes may affect viscoelastic properties of the film and, hence, changes of dynamic resistance of the quartz resonator, ΔR. Therefore, in a 15-scan CV experiment we simultaneously measured current, resonant frequency change, and dynamic resistance change as a function of potential.

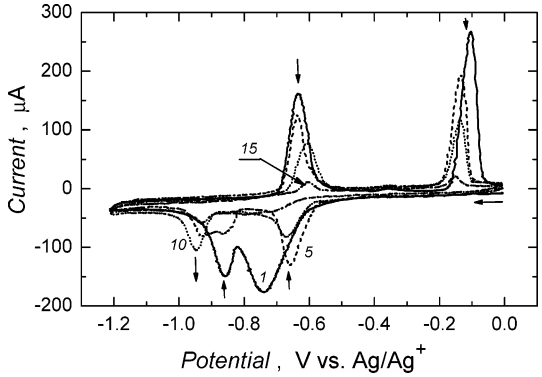

Figure 5. Multiscan cyclic voltammogram for the C_{60} film in 0.1 M $(TBA)PF_6$, in acetonitrile. After initial aggregation for 1 min, the film was electrophoretically deposited for 3 min at 50 V dc in a mixed solvent solution of a toluene-to-ethanol ratio of 1:10 (v/v) on a 10-MHz Pt/quartz electrode. Cycle number is indicated at each curve. Potential sweep rate was 0.1 V s^{-1}.

It appeared that electrochemical properties of C_{60} films were independent of the aggregation time. Therefore, results for a C_{60} film of ca. 45 nm average thickness (52 equivalent monolayers), deposited for 3 min at 50 V dc after the initial 1 min aggregation in solution, are presented below.

The multiscan CV behavior (Figure 5) was very distinctive in that the dependence of current, the resonant frequency change, and the dynamic resistance change on potential of cycle 1 was markedly different from those of subsequent cycles. That is, in cycle 1, two cathodic peaks, corresponding to the C_{60}^0/C_{60}^- and C_{60}^-/C_{60}^{2-} electroreductions, were observed at −0.74 and −0.86 V, respectively. The first cathodic peak was much larger and broader than the second one (Figure 5, cycle 1). In that respect, this CV behavior was, on one hand, qualitatively similar to that displayed by C_{60} films prepared by electrochemical deposition, abrasive attachment, or solution casting[14,15,70] and, on the other hand, different from that revealed by the fullerene films prepared by sublimation (where only one broad peak for the merged first two cathodic peaks was observed)[18] and that characteristic for fullerenes embedded in the electrode surface-confined membranes (where reversible redox behavior of the first three electroreductions was observed).[51−60] Then two related anodic peaks at −0.63 and −0.10 V were recorded after reversal of the potential scan. In cycle 2, the first

(66) Tatsuma, T.; Kikuyama, S.; Oyama, N. *J. Phys. Chem.* **1993**, *97*, 12067.
(67) Zhou, F.; Yau, S.-L.; Jehoulet, C.; Laude, J., D. A.; Guan, Z.; Bard, A. J. *J. Phys. Chem.* **1992**, *96*, 4160.
(68) Szücs, Á.; Loix, A.; Nagy, J. B.; Lamberts, L. *J. Electroanal. Chem.* **1996**, *402*, 137.
(69) Szucs, A.; Novak, M. *J. Solid State Electrochem.* **2005**, *9*, 304.
(70) Chlistunoff, J.; Cliffel, D.; Bard, A. J. Charge-transfer Salts, Fullerenes and Photoconductors. In *Handbook of Conductive Molecules and Polymers*; Nalwa, H. S., Ed.; Wiley: Chichester, U.K., 1997; Vol. 1, Chapt. 7, pp 333−412.

cathodic peak was shifted positively to −0.66 V as if the C_{60}^0/C_{60}^- electroreduction became less energy-demanding. Interestingly, the potential of the second cathodic peak was not altered but its height decreased and a current shoulder appeared on its tail. In the subsequent 14 cycles, the first cathodic peak decreased along with the two anodic peaks. However, the second cathodic peak decreased at the expense of the increase of a new cathodic peak at more negative potential, that is, at −0.95 V. In effect, the original second cathodic peak disappeared completely after about 10 cycles and only the new peak was left, thus indicating some structural transformations in the film. Then, during cycles 11−15, this new cathodic peak decreased along with all other peaks, pointing to slow dissolution of the film during each potential cycle.

From the slope of the rising portion of current of the first cathodic peak of cycle 1, at the peak half-height, $E_{pc/2}$, apparent redox conductivity, $\Lambda = (d/A)(\Delta i/\Delta E)_{E=E_{pc/2}}$,[71] of the film was determined. From our AFM investigations (see section 3.2), it follows that surface coverage and effective thickness of the surface domains for this film were ca. 50% and 500 nm, respectively. Hence, the redox conductivity is $\Lambda \approx 4.3 \times 10^{-5}$ S m^{-1}, being practically invariant with respect to the film thickness. This value is lower than that of a vapor-deposited C_{60} film partially doped electrochemically with TBA^+,[72] and such films electrochemically doped with $M(bpy)_3^{2+}$ (M = Fe, Ni, Ru, or Os; bpy = 2,2′-bipyridine),[73] or of the one synthesized by electrocrystallizaton of $Ru(bpy)_3 \times (C_{60})_2$ salt.[74] These conductivity differences may arise from different hindrance of counterion diffusion in films of different morphology.

Evolution of the piezoelectric microgravimetric behavior accompanying multiscan CV performance is presented in Figure 6. The behavior revealed in cycle 1 (Figure 6) was markedly different than that of subsequent cycles. The first cathodic peak was accompanied by a negative peak in the Δf vs E trace at −0.73 V (center curve in Figure 6, cycle 1) and a positive peak in the ΔR vs E trace at −0.75 V (bottom curve in Figure 6, cycle 1). Notably, the Δf vs E curve was different for the electrophoretically deposited C_{60} film examined here from that reported earlier for electrochemically deposited C_{60} film where Δf vs E steps rather than peaks were observed.[32] The frequency decrease with the increase of current of the first and second cathodic peak can be ascribed both to the mass increase of the film due to the ingress of TBA^+ for compensation of the negative charge of C_{60}^- and C_{60}^{2-} produced, respectively, and to the change of viscoelastic properties of a contacting medium:[75]

$$\Delta f = -f_0^{3/2}\left(\frac{\eta_L \rho_L}{\pi \mu_Q \rho_Q}\right)^{1/2} \quad (2)$$

where η_L and ρ_L are dynamic viscosity and density, respectively, of the contacting liquid. Then, the total frequency shift for the mass-loaded quartz resonator immersed in a viscous medium is the sum of eqs 1 and 2:

$$\Delta f = -\left[\frac{2f_0^2}{(\mu_Q \rho_Q)^{1/2}}\right]\left[\left(\frac{\Delta m}{A}\right) + \left(\frac{\eta_L \rho_L}{4\pi f_0}\right)^{1/2}\right] \quad (3)$$

Therefore, it is impossible to determine contribution to the total frequency change originating from the mass change component and the viscoelasticity change component from the sole measurement of the frequency change. Independent simultaneous measurements of a variable related to viscoelasticity of ambient, like dynamic resistance of the quartz resonator, R,[75] are necessary for that purpose:

$$R = \frac{A}{k^2}(2\pi f_0 \eta_L \rho_L)^{1/2} \quad (4)$$

(where $k^2 = 7.74 \times 10^{-3}$ A^2 s m^{-2} is the electromechanical coupling factor for the quartz resonator). Hence, from equations (2) and (4) it follows that the frequency change is opposite to the dynamic resistance:

$$\Delta f = -\frac{k^2 R f_0}{\pi A (2\mu_Q \rho_Q)^{1/2}} \quad (5)$$

Qualitatively, the considerations involving quartz resonator in contact with viscous liquid can be extended to viscous film coats. Then the simultaneous ΔR increase and Δf decrease, associated with the current at the foot of the first cathodic peak observed in the present work, may be interpreted in terms of both initial mass increase due to the TBA^+ ingress and swelling of the film with the solvent. At potentials of the tail of the first cathodic peak, frequency increases (center curve in Figure 6, cycle 1) accompanied by a decrease in the dynamic resistance. This behavior may originate from at least two effects. That is, it may arise from some additional rigidity gained by the film induced by inserted TBA^+ cation or egress of the PF_6^- anion (see below in section 3.5), which results in a net mass loss of the film. The second cathodic peak is accompanied by the Δf decrease because more TBA^+ enters the film for charge neutralization of C_{60}^{2-} generated. In effect, the film becomes, presumably, even more rigid because ΔR mildly decreases at potentials of the tail of the second cathodic peak.

The charge associated with the C_{60}^{2-}/C_{60}^- and C_{60}^-/C_{60}^0 electrooxidation, determined by integration of anodic peak currents, is equal to 250 and 290 μC, respectively. However, the frequency step associated with the C_{60}^{2-}/C_{60}^- electrooxidation, $\Delta f_{2-/-} = 972$ Hz, is much higher than that associated with the C_{60}^-/C_{60}^0 peak, $\Delta f_{-/0} = 139$ Hz (center curve in Figure 6, cycle 1). Most likely, the former step is additionally due to loss of solvent and ions of the supporting electrolyte. This loss might be responsible for the positive peak at −0.61 V in the ΔR vs E trace (bottom curve in Figure 6, cycle 1).

(71) Pickup, P. G.; Kutner, W.; Leidner, C. R.; Murray, R. W. *J. Am. Chem. Soc.* **1984**, *106*, 1991.
(72) Nishizawa, M.; Matsue, T.; Uchida, I. *J. Electroanal. Chem.* **1993**, *353*, 329.
(73) Nishizawa, M.; Tomura, K.; Matsue, T.; Uchida, I. *J. Electroanal. Chem.* **1994**, *379*, 233.
(74) Foss, C. A.; Feldheim, D. L.; Lawson, D. R.; Dorhout, P. K.; Elliott, C. M.; Martin, C. R.; Parkinson, B. A. *J. Electrochem. Soc.* **1993**, *140*, L84.
(75) Thompson, M.; Kipling, A. L.; Duncan-Hewitt, W. C.; Rajakoviæ, L. V.; Èaviæ-Vlasak, B. A. *Analyst* **1991**, *116*, 881.

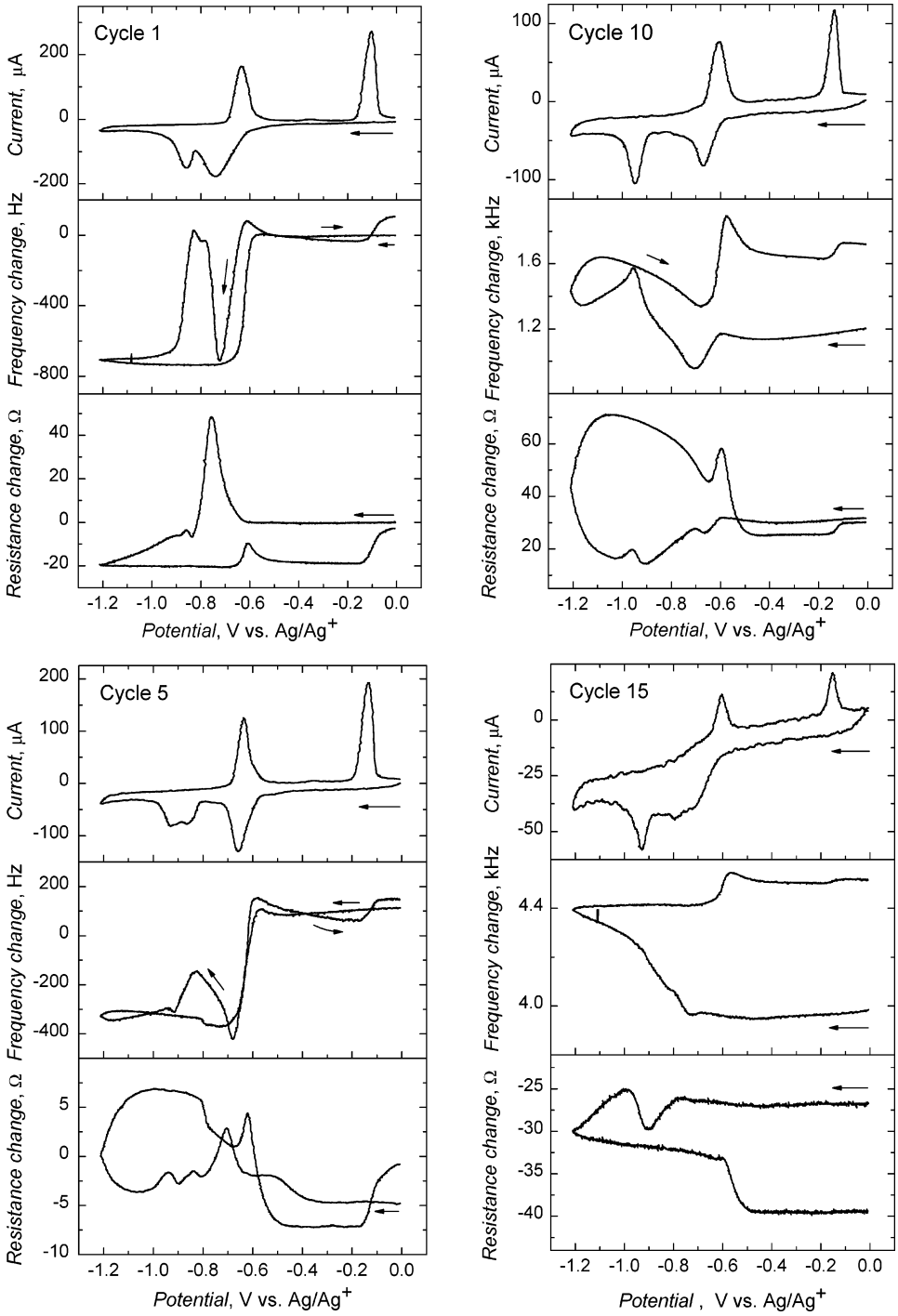

Figure 6. Simultaneously recorded traces of the multiscan cyclic voltammogram (top), resonant frequency change vs potential (center), and dynamic resistance change vs potential (bottom) for the C_{60} film in 0.1 M (TBA)PF_6, in acetonitrile. After initial aggregation for 1 min, the film was electrophoretically deposited for 3 min at 50 V dc in a mixed solvent solution of a toluene-to-ethanol ratio of 1:10 (v/v) on a 10-MHz Pt/quartz electrode. Cycle number is indicated in each panel. Potential sweep rate was 0.1 V s^{-1}.

That is, the initial ΔR rise of this peak may originate from the initial viscoelasticity gain by the film in the course of the initial TBA^+ egress. The subsequent decrease of ΔR points to the increase of the film rigidity as further amounts of TBA^+ and, presumably, solvent are expelled. The ΔR vs E positive step corresponding to the C_{60}^-/C_{60}^0 CV anodic peak is much higher than the above-described peak in the ΔR vs E curve corresponding to the C_{60}^{2-}/C_{60}^- anodic peak. It could be that the negative contribution of the viscoelastic changes to the overall frequency changes of the Δf vs E step is higher at more positive potentials. Therefore, the frequency step at more positive potentials is lower than that at more negative ones.

In cycle 5, in both the Δf vs E (center curve in Figure 6, cycle 5) and ΔR vs E (bottom curve in Figure 6, cycle 5) transients, there are negative and positive, respectively, peaks present associated with the first cathodic peak. This behavior is similar to that for cycle 1 except that tails of the respective peaks are higher. The second cathodic peak is split. This peak is accompanied by the Δf decrease and two positive ΔR peaks as if TBA^+ ingress were accompanied by solvent exchange, leading to changes in viscoelasticity of the film.

Then, at potentials more negative than −1.15 V, Δ*R* increases in the course of both initial negative and subsequent positive potential scanning. Qualitatively, the Δ*f* vs *E* and Δ*R* vs *E* behavior of the anodic scan is similar to that of cycle 1, but for cycle 5 the positive peak in the Δ*R* vs *E* curve corresponding to the C_{60}^{2-}/ C_{60}^{-} anodic peak is twice as high as the positive step in the Δ*R* vs *E* curve corresponding to the C_{60}^{-}/C_{60}^{0} anodic peak.

In cycle 10, the Δ*f* vs *E* and Δ*R* vs *E* transients are very much different than those in cycle 1 (Figure 6. Although the first cathodic peak is accompanied by the negative peak in the Δ*f* vs *E* curve and a small positive peak in the Δ*R* vs *E* curve, the second cathodic peak is associated with a positive peak in both the Δ*f* vs *E* and Δ*R* vs *E* curves.

Finally, in cycle 15, the Δ*f* vs *E* and Δ*R* vs *E* transients are completely different than those in cycle 1 (Figure 6). That is, there is a continuous decrease of Δ*f* in the negative scan at potentials more negative than those of the first cathodic peak, and a negative peak in the Δ*R* vs *E* curve accompanies the second but not the first cathodic peak. In the anodic sweep, the C_{60}^{2-}/C_{60}^{-} and C_{60}^{-}/C_{60}^{0} anodic peak is accompanied by a positive peak and step, respectively, in the Δ*f* vs *E* curve. Interestingly, a negative step in the Δ*R* vs *E* curve is associated only with the C_{60}^{2-}/ C_{60}^{-} but not the C_{60}^{-}/C_{60}^{0} anodic peak.

Apparent ion crossing of the film−solution interface can be quantitatively estimated by examining the mass on charge dependence for redox processes occurring in films. For that purpose, curves of the frequency change versus charge were plotted in Figure 7. These curves were recalculated from curves of the current and frequency change vs potential for different CV cycles shown in Figure 6. From slopes of the raising portions of these curves, corresponding to potentials of the foot of the first cathodic peak, values of the apparent electrochemical equivalent of the counterion entering the film were determined by invoking the Faraday law and the Sauerbrey equation (eq 1). For cycles 1, 5, and 10, these values were close to 588, 513, and 256 g/mol. Since the molecular weights are, MW(TBA^+) = 242.45 and MW(PF_6^-) = 144.95, one may postulate for this mass gain one TBA^+ counterion and, additionally, around one half $TBA^+-PF_6^-$ ion pair entering the film per one C_{60}^{-} anion generated in cycle 1. A decrease of the apparent electrochemical equivalent with the cycle number indicates the increase of some hindrance for ions of the supporting electrolyte to cross the film−solution interface under dynamic CV conditions. Most likely, the $TBA^{+-}PF_6^-$ ion pair is eventually retained in both the electroreduced and electrooxidized films. However, ions of the supporting electrolyte are expelled completely from the film under constant-potential exhaustive C_{60}^{-}/C_{60}^{0} electrooxidation (see below in section 3.5).

3.4. Electrochemical Dissolution of Electrophoretically Deposited C_{60} Films. Four main cathodic peaks, corresponding to four one-electron reductions, are present in the CV curve for the electrophoretically deposited C_{60} film during the negative potential excursion covering the entire accessible potential window of the acetonitrile solvent solution (Figure 8). Behavior of the first two peaks is described above (see section 3.3). Similar to the CV behavior of the electrochemically deposited C_{60} film,[32] the third cathodic peak, corresponding to the C_{60}^{2-}/C_{60}^{3-} electroreduction, is split. An abrupt frequency increase at −1.40 V accompanying this peak is due to a dramatic mass drop, which indicates complete dissolution of the film. Elevated current of the more negative part of the third cathodic peak may arise from electroreduction of dissolved C_{60}^{2-}. Further negative polarization does not alter Δ*f* as the fourth cathodic peak at ca. −1.80 V, corresponding to the solution C_{60}^{3-}/C_{60}^{4-} redox

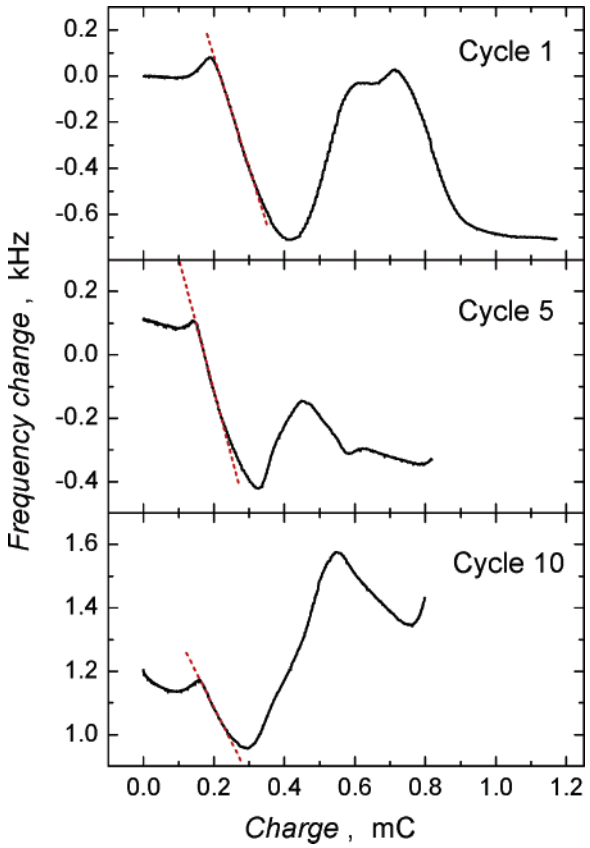

Figure 7. Dependence of frequency changes on charge. Data were recalculated from the CV and the frequency change vs potential curves shown in Figure 6. Number of CV cycle is indicated at each curve.

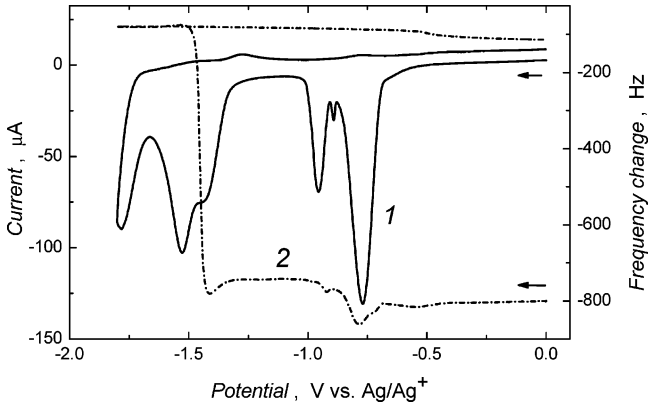

Figure 8. Simultaneously recorded (1) cyclic voltammogram and (2) resonant frequency change vs potential for the C_{60} film in 0.1 M $(TBA)PF_6$, in acetonitrile. After initial aggregation for 1 min, the film was electrophoretically deposited for 12 min at 50 V dc in a mixed solvent solution of a toluene-to-ethanol ratio of 1:10 (v/v) on a 5 MHz Pt/quartz electrode. Potential sweep rate was 0.1 V s^{-1}.

couple, is produced. In the positive half cycle, the anodic peaks are hardly visible because the dissolved fullerene anions diffuse away from the electrode surface.

3.5. Compositional and Structural Aspects of the Neutral, Electroreduced, and Subsequently Back-Electrooxidized C_{60} Films. Both the XPS and powder XRD analyses were performed on C_{60} films, which were (i) freshly deposited by electrophoresis onto a Pt/quartz resonator; then (ii) exhaustively electroreduced at potential more negative by ca. 0.1 V than that of the first, C_{60}^0/C_{60}^-, cathodic peak to form a C_{60}^- film; and finally (iii) exhaustively electrooxidized back at potential more positive by 0.1 V than that of the C_{60}^-/C_{60}^0 anodic peak to form a C_{60}^0 film again.

The XPS analysis of the C_{60} films provided some information on the film elemental composition. That is, first, a freshly deposited C_{60} film revealed (not shown) typical low-energy π-type shake-up satellites located on the high binding energy side of the C 1s spectrum of fullerene, similarly as for a C_{60} film prepared by physical vapor deposition.[20] Then, a mole ratio of C_{60}:TBA^+:PF_6^- $\approx$ 1:2:1 was determined for the electroreduced film from the relative integrated intensities of the respective C 1s, N 1s, F 1s, and P 2p core level spectra. This result, in quantitative agreement with that obtained from piezoelectric microgravimetric measurements (see section 3.3), indicates that the charge of each C_{60}^- anion generated in the film was compensated by one TBA^+ cation and, additionally, one pair of $(TBA)^+$ and PF_6^- ions entered the film per one C_{60}^- generated. That is, the amount of incorporated TBA^+-PF_6^- ion pair was higher under the exhaustive electrolysis rather than CV conditions. Finally, no $(TBA)PF_6$ was detected in the electrooxidized film. Apparently, $(TBA)PF_6$ was removed from the film when the fullerene anion lost its negative charge in the effect of electrooxidation. Additionally, signals of oxygen ($\sim$20 at. %), silicon ($\sim$10 at. %), and platinum ($\sim$4 at. %) were detected in all samples that originated from the Pt/quartz resonator support.

The XRD pattern of a freshly deposited C_{60} film revealed (curve 1 in Figure 9) three peaks at scattering angles of 10.95°, 17.85°, and 20.87°, typical for C_{60} crystallites of face-centered cubic (fcc) packing.[17,73,76,77] A small shift of the peak positions toward larger angles originated, most likely, from imperfect alignment of a resonator plane with respect to a goniometer axis. After applying the Scherrer equation[78] to half-widths of the peaks, one may conclude that either mean diameter of the C_{60} crystallites is 15 nm or, if lattice strain is high, the distance at which correlations between atom locations disappear is 15 nm.

Exhaustive C_{60}/C_{60}^- electroreduction in the film resulted in a complex XRD pattern (curve 2 in Figure 9). As described above (see above sections 3.3 and 3.4), both TBA^+ and PF_6^- ion enters the film during this electroreduction. Therefore, for comparison, a XRD pattern was recorded for a (TBA)-PF_6 film prepared by drop coating from the acetonitrile solution onto a Pt/quartz resonator. The pattern obtained (curve 3 in Figure 9) displays peaks that fit well to those described in the literature.[79] Because the pattern intensity for the electroreduced fullerene film was much higher than that for the freshly deposited film, with its background resembling that of the latter, we concluded that the strong peaks recorded are due to the formation of some crystalline phase external to the fullerene phase. These peaks can be linked, in accord with our piezoelectric microgravimetric and XPS results, to crystallites of the $(TBA)PF_6$ salt indicating its presence in the film, as opposed to its absence in the electroreduced C_{60} film deposited by sublimation.[17] Apparently, the acetonitrile solution containing both TBA^+ and PF_6^- ions readily entered the electrophoretically deposited porous fullerene film during C_{60}^0/C_{60}^- electroreduction and the solid $(TBA)PF_6$ salt remained in its crystalline form after solvent evaporation. The diameter of the resulting crystallites, estimated from half-widths of the $(TBA)PF_6$ peaks, was close to 50 nm. The peaks characteristic for the $(TBA)PF_6$ nanocrystallites were absent in the pattern recorded for the electroreduced fullerene film extensively rinsed with deaerated acetonitrile. Apparently, the $(TBA)PF_6$ solid was then completely washed away.

After subsequent exhaustive back electrooxidation of the reduced film of C_{60}^- to C_{60}^0, peaks seen in a pattern characteristic of C_{60}^- (curve *2* in Figure 9) disappeared and the obtained pattern featured, in accord with earlier results,[17,73,76,77] three broad peaks (curve 4 in Figure 9) at

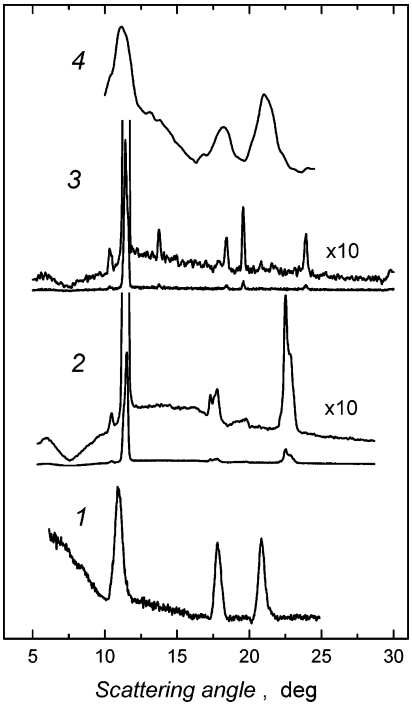

Figure 9. Powder XRD patterns for (1) the C_{60} film freshly deposited on a Pt/quartz electrode by electrophoresis; (2) the C_{60} film electroreduced to C_{60}^- at -0.8 V in 0.1 M $(TBA)PF_6$, in acetonitrile, for 2 min; (3) the $(TBA)PF_6$ film deposited on a Pt/quartz electrode by evaporation from acetonitrile solution; and (4) the C_{60}^- film reoxidized to C_{60}^0 at 0.1 V in 0.1 M $(TBA)PF_6$, in acetonitrile, for 2 min.

(76) JCPDS Data File 85-1799; International Centre for Diffraction Data: Philadelphia PA, 1999.
(77) Hebard, A. F.; Haddon, R. C.; Fleming, R. M.; Kortan, A. R. *Appl. Phys. Lett.* **1991**, *59*, 2109.
(78) Huber, C. A. In *Handbook of Nanophase Materials*; Goldstein, A. N., Ed.; Marcel Dekker: New York, 1997.
(79) JCPDS Data File 46-1802; International Centre for Diffraction Data: Philadelphia PA, 1999.

scattering angles of 11.2°, 18.1°, and 21.1°, thus pointing to the presence of C_{60} crystallites of the fcc packing. That is, the structure of the initial film was regained. The difference, however, was in the coherently dispersing areas (calculated from peak half-widths), which decreased to 7−9 nm as if the C_{60} crystallite diameter was decreased almost by half as compared to that of the C_{60} crystallites of the freshly deposited film. Moreover, this diameter is even smaller than that of vapor-deposited C_{60} film determined after reversible ingress and egress of $M(bpy)_3^{2+}$ cation upon sequential exhaustive C_{60}^0/C_{60}^- electroreduction and electrooxidation, respectively.[73] Interestingly, there were no peaks corresponding to the $(TBA)PF_6$ salt in this spectrum. Most likely, the exhaustive C_{60}^-/C_{60}^0 electrooxidation led to a complete expulsion of the supporting electrolyte ions and resulted in a pristine C_{60} hydrophobic film, in accord with our XPS results (see above in this section).

4. Conclusions

By bulk electrophoresis, relatively rough nanocrystalline fullerene films of controlled surface topography, featuring nonfractal spheroidal surface structures can be prepared. The experimental control over three-dimensional surface assembling of fullerene clusters was gained by suitably adjusting conditions of electrophoretic deposition. That is, for the same dc voltage applied, films of higher surface roughness were obtained for shorter rather than longer aggregation time although the size of the deposited aggregates was virtually the same. The aggregate size in films was larger for higher dc voltage applied. Piezoelectric microgravimetric monitoring allowed us for both qualitative and quantitative characterization of the rate of the electrophoretic fullerene deposition, which has not been accomplished earlier.

Exhaustive C_{60}^-/C_{60}^0 electroreduction was accompanied by both TBA^+ counterion and PF_6^- co-ion ingress into the film. Subsequent exhaustive C_{60}^-/C_{60}^0 electrooxidation resulted in a complete removal of both cations and anions of the supporting electrolyte from the film. This reversible ion doping was similar to that of other ions reported earlier.[17,73] Taken into account for the first time in the present study, viscoelastic effects accompanying electrochemical processes affected considerably the microgravimetric behavior of electrophoretically deposited fullerene films.

Similar to the C_{60} films prepared by other deposition procedures, the electrophoretically deposited C_{60} films appeared to be very unstable with respect to dissolution in the acetonitrile solutions at potentials corresponding to the formation of C_{60}^{3-} anion.

Experimental control over three-dimensional surface assembling of fullerene clusters in films, demonstrated in the present study, opens up new avenues to design high-surface-area electrode materials of potential use in, for instance, portable fuel cells, chemical sensors, and light-energy converting devices. Such studies on both pristine and functionalized fullerene-based nanostructured electrodes are in progress in our laboratories.

Acknowledgment. Financial support from the State Committee for Scientific Research of Poland, Project 4 T09A 160 23 (to W.K.), the National Science Foundation, and the Petroleum Research Fund administered by the American Chemical Society (to F.D.) are gratefully acknowledged.

CM050829I